Influence of flexoelectricity on electrohydrodynamic instabilities in nematics

N. V. Madhusudana[a]; V. A. Raghunathan[a]

[a] Raman Research Institute, Bangalore, India

PLEASE SCROLL DOWN FOR ARTICLE

Influence of flexoelectricity on electrohydrodynamic instabilities in nematics

by N. V. MADHUSUDANA and V. A. RAGHUNATHAN

Raman Research Institute, Bangalore 560080, India

We have incorporated the flexoelectric terms in developing one-dimensional models of E.H.D. instabilities in nematics both under D.C. and A.C. excitations. It is shown that, using this model, we can account for the following experimental observations, which could not be adequately explained by earlier models: (i) The observation of oblique rolls whose wave vector **q** makes an angle α with the undistorted director $\mathbf{n}_0$, up to some frequency v_0 in the conduction regime; (ii) the oblique rolls found in the dielectric regime; and (iii) the 'longitudinal' E.H.D. instabilities in some systems with negative conductivity anisotropy. We also present some experimental observations under D.C. excitation.

1. Introduction

The electrohydrodynamic instabilities exhibited by nematics with negative or weakly positive dielectric anisotropy and positive conductivity anisotropy are well understood in terms of the Helfrich [1] and Orsay [2, 3] models. However, there are some aspects of these instabilities that cannot be understood using these models:

(i) the observation of oblique rolls whose wave vector **q** makes an angle with the undistorted director $\mathbf{n}_0$, up to a frequency v_0 in the conduction regime [4];

(ii) the chevron pattern observed slightly above the threshold in the dielectric regime, in which the wave vector of the rolls makes an angle with $\mathbf{n}_0$ [5];

(iii) *the E.H.D. instabilities observed in nematics with negative conductivity anisotropy [6, 7].*

We have recently shown [8–10] that the above observations can be accounted for by incorporating flexoelectricity [11] in the theory of E.H.D. instabilities. Flexoelectricity influences the problem in two ways. First, the action of the total electric field in the medium on the flexoelectric polarization [11]

$$\mathbf{P} = e_1 \mathbf{n} \nabla \cdot \mathbf{n} + e_3 (\nabla \times \mathbf{n}) \times \mathbf{n} \qquad (1)$$

leads to an additional torque on the director. Secondly, **P** contributes to the space-charge density Q in the medium, given by

$$\nabla \cdot \mathbf{D} = 4\pi Q, \qquad (2)$$

where

$$\mathbf{D} = \varepsilon_\perp \mathbf{E} + \Delta\varepsilon (\mathbf{n} \cdot \mathbf{E})\mathbf{n} + 4\pi \mathbf{P} \qquad (3)$$

is the displacement vector. In this paper we present the detailed results of a one-dimensional linear analysis [8, 10] that takes into account the flexoelectric terms. The theoretical results are compared with experimental observations.

2. The electrohydrodynamic equations

Consider a homogeneously aligned nematic layer lying in the (X, Y) plane with the director $\mathbf{n}_0$ along the X axis. Under the action of an electric field $\mathbf{E}_0$ applied along Z, we assume that the E.H.D. instability gives rise to oblique rolls whose wave vector $\mathbf{q}$ lies along ξ, making an angle α with $\mathbf{n}_0$ (figure 1). In the deformed state $\mathbf{n}$ makes polar angles θ and ϕ in the (X, Y, Z) system, so that the components of $\mathbf{n}$ in the (ξ, η, Z) system are $[\cos \theta \cos (\alpha - \phi), \ -\cos \theta \sin (\alpha - \phi), \ \sin \theta]$. Since the boundary conditions are neglected, only the Z component of the velocity $\mathbf{v}$ appears in the equations. The transverse field created in the medium due to the space charges has, by symmetry, only a ξ component E_ξ. Further, v_z, θ, ϕ and E_ξ are assumed to be functions of ξ alone.

The system is described by the following equations.

(i) *The Poisson equation*: $\nabla \cdot \mathbf{D} = 4\pi Q$. Substituting for $\mathbf{D}$ from (3), we get

$$4\pi Q = \varepsilon_c \frac{\partial E_\xi}{\partial \xi} + \Delta \varepsilon \, E_0 c \, \frac{\partial \theta}{\partial \xi} + 4\pi(e_1 + e_3)sc \, \frac{\partial^2 \phi}{\partial \xi^2}, \qquad (4)$$

where $\varepsilon_c = \varepsilon_\perp + \Delta \varepsilon \, c^2$, $s = \sin \alpha$ and $c = \cos \alpha$.
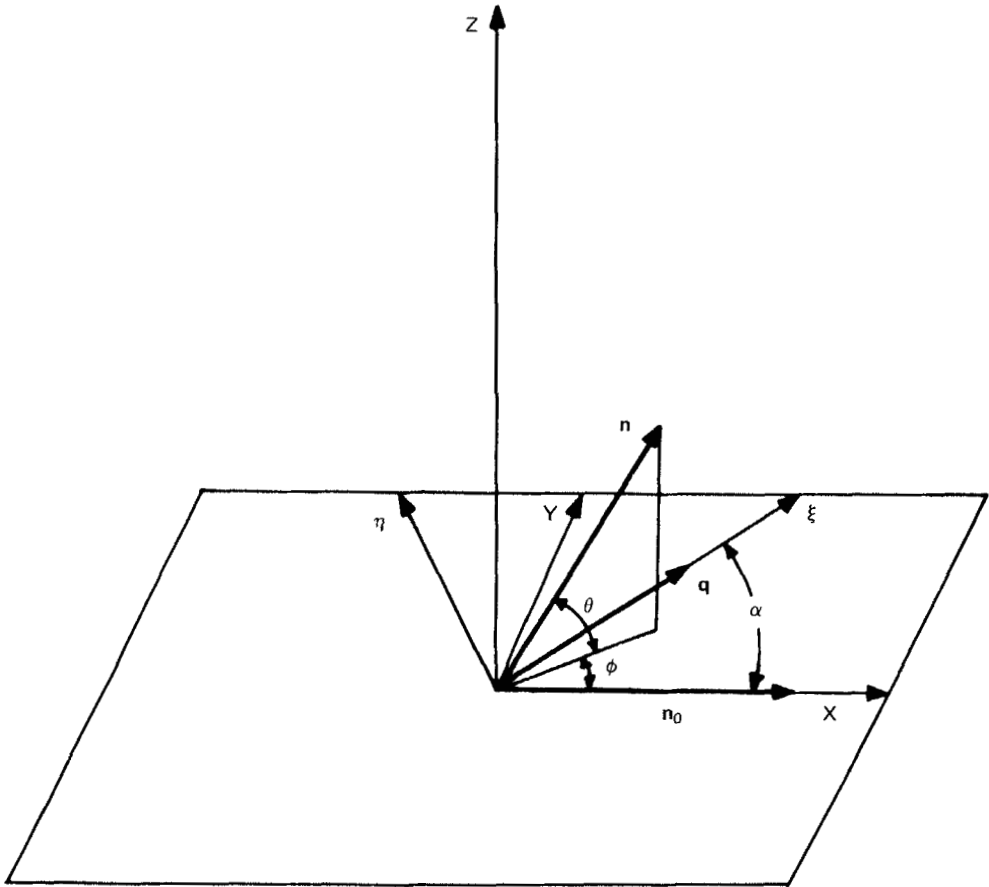

Figure 1. Coordinate system and definitions of angles used in the text.

(ii) *The charge conservation equation*: $\partial Q/\partial t + \nabla \cdot \mathbf{J} = 0$, where $\mathbf{J} = \sigma_\perp \mathbf{E} + \Delta\sigma(\mathbf{n} \cdot \mathbf{E})\mathbf{n}$. From these, we get

$$\frac{\partial Q}{\partial t} + \sigma_c \frac{\partial E_\xi}{\partial \xi} + \Delta\sigma E_0 c \frac{\partial \theta}{\partial \xi} = 0 \qquad (5)$$

where $\sigma_c = \sigma_\perp + \Delta\sigma c^2$.

(iii) *The equation of motion*, following the notation of [2], is given by

$$\varrho \frac{\partial \mathbf{v}}{\partial t} + \text{div}(\varrho \mathbf{vv}) - \text{div}(\boldsymbol{\sigma} + \boldsymbol{\sigma}') = Q\mathbf{E},$$

where ϱ is the density, $\boldsymbol{\sigma}$ the elastic stress tensor and $\boldsymbol{\sigma}'$ the viscous stress tensor. The inertial term in the above equation is negligible as long as the frequency of the applied field is not too large [2]. Further, $\boldsymbol{\sigma}$ does not lead to any linear terms in θ and ϕ. Neglecting the inertial and non-linear terms in the above equation and substituting for $\boldsymbol{\sigma}'$, the following equation is obtained:

$$\alpha_2 c \frac{\partial \dot\theta}{\partial \xi} + \eta_1 \frac{\partial^2 v_z}{\partial \xi^2} + QE_0 = 0, \qquad (6)$$

where

$$\dot\theta = \frac{\partial \theta}{\partial t}, \qquad \eta_1 = \tfrac{1}{2}[\alpha_4 + (\alpha_5 - \alpha_2)c^2],$$

where α_i are the Leslie viscosity coefficients.

(iv) *The torque-balance equation*:

$$\Gamma_i^{\text{elastic}} + \Gamma_i^{\text{dielec}} + \Gamma_i^{\text{flexo}} = \Gamma_i^{\text{hydrodyn}}, \quad i = Y, Z.$$

Substituting for these terms, the following equations are obtained for the torque balance along Y and Z respectively:

$$\gamma_1 \dot\theta + \alpha_2 c \frac{\partial v_z}{\partial \xi} - M \frac{\partial^2 \theta}{\partial \xi^2} - \frac{\Delta\varepsilon}{4\pi} E_0^2 \theta - \frac{\Delta\varepsilon}{4\pi} E_0 c E_\xi - (e_1 - e_3)E_0 s \frac{\partial \phi}{\partial \xi} = 0, \qquad (7)$$

$$\gamma_1 \dot\phi + (e_1 - e_3)s E_0 \frac{\partial \theta}{\partial \xi} - L \frac{\partial^2 \phi}{\partial \xi^2} + (e_1 + e_3)s c \frac{\partial E_\xi}{\partial \xi} = 0, \qquad (8)$$

where $\dot\phi = \partial\phi/\partial t$, $M = K_2 s^2 + K_3 c^2$, $L = K_1 s^2 + K_3 c^2$, and K_1, K_2 and K_3 are the splay, twist and bend elastic constants respectively.

3. D.C. excitation

In the case of D.C. excitation the time dependence in the above equations can be neglected since we confine our attention to stationary solutions. Eliminating v_z, E_ξ and Q from the above relations, we get the following two equations in θ and ϕ:

$$L \frac{d^2 \phi}{d\xi^2} - (e_1 - e_3)E_0 s \frac{d\theta}{d\xi} + (e_1 + e_3)\sigma_R E_0 s c^2 \frac{d\theta}{d\xi} = 0, \qquad (9)$$

$$M \frac{d^2 \theta}{d\xi^2} + \left[(e_1 - e_3) + \frac{\alpha_2}{\eta_1}(e_1 + e_3)c^2 \right] E_0 s \frac{d\phi}{d\xi}$$
$$+ \left[\frac{\Delta\varepsilon}{4\pi} \frac{\sigma_\perp}{\sigma_c} + \frac{\alpha_2}{\eta_1} \frac{\varepsilon_c}{4\pi}(\varepsilon_R - \sigma_R)c^2 \right] E_0^2 \theta = 0, \qquad (10)$$

Material parameters of MBBA.

$K_1 = 6\cdot1 \times 10^{-7}$ dyn	$\alpha_1 = 6\cdot5$ cP	$\sigma_\parallel = 1\cdot0 \times 10^{-10}$ ohm^{-1} cm^{-1}
$K_2 = 4\cdot0 \times 10^{-7}$ dyn	$\alpha_2 = -77\cdot5$ cP	
$K_3 = 7\cdot3 \times 10^{-7}$ dyn	$\alpha_3 = -1\cdot2$ cP	$\dfrac{\Delta\sigma}{\sigma_\perp} = 0\cdot5$
$\varepsilon_\parallel = 4\cdot7$	$\alpha_4 = 83\cdot2$ cP	$e_1 - e_3 = 1\cdot2 \times 10^{-4}$ c.g.s. units
$\varepsilon_\perp = 5\cdot2$	$\alpha_5 = 46\cdot3$ cP	$e_1 + e_3 = -7\cdot0 \times 10^{-4}$ c.g.s. units

where $\varepsilon_R = \Delta\varepsilon/\varepsilon_c$ and $\sigma_R = \Delta\sigma/\sigma_c$. The above equations clearly admit solutions of the form $\theta = \theta_0 \sin q\xi$ and $\phi = \phi_0 \cos q\xi$. Substituting these solutions into (9) and (10), the following relation between E_0 and q is obtained:

$$E_0^2 = \frac{MLq^2}{\left[\dfrac{\Delta\varepsilon\,\sigma_\perp}{\sigma_c} + \dfrac{\alpha_2}{\eta_1}\varepsilon_c(\varepsilon_R - \sigma_R)c^2\right]\dfrac{L}{4\pi} + Fs^2}, \tag{11}$$

where

$$F = (e_1 - e_3)^2 - (e_1 + e_3)^2\frac{\sigma_R\alpha_2}{\eta_1}c^4 + (e_1^2 - e_3^2)\left(\frac{\alpha_2}{\eta_1} - \sigma_R\right)c^2.$$

If we now assume, as in the Helfrich model [1], that $q = \pi/d$, where d is the sample thickness, then (11) gives a voltage threshold

$$V_{th}^2 = \frac{ML\pi^2}{\left[\dfrac{\Delta\varepsilon\,\sigma_\perp}{\sigma_c} + \dfrac{\alpha_2}{\eta_1}\varepsilon_c(\varepsilon_R - \sigma_R)c^2\right]\dfrac{L}{4\pi} + Fs^2}. \tag{12}$$

For a given set of values of the material parameters the threshold voltage V_{th} can be calculated for different values of the angle α. The lowest value of V_{th} gives the critical voltage V_c for the onset of the instability, and the corresponding value of α gives the tilt of the rolls at the threshold. The variation of V_{th} with α, calculated for the standard values of the material parameters of MBBA (listed in the table), is shown in figure 2. For this case the instability sets in at a critical voltage of $1\cdot715$ V with $\alpha = 0\cdot83$ rad.

From (9) we find that in the absence of the ϕ distortion $\alpha = 0$. In other words, the ϕ distortion is essential for the production of oblique rolls. In the absence of the ϕ distortion the system cannot differentiate between domains with $+\alpha$ and those with $-\alpha$, and for physical reasons chooses $\alpha = 0$. However, when there is a non-zero ϕ, the relative signs of θ_0 and ϕ_0 depend on the sign of α for any given sign of E.

If the flexoelectric terms are neglected, it follows from (9) and (10) that there cannot be a ϕ distortion of the director field, and hence $\alpha = 0$. Thus in the context of a one-dimensional model the flexoelectric terms are entirely responsible for the oblique rolls. In order to clearly understand the influence of these terms, let us simplify the problem by taking $\Delta\varepsilon = 0$ and $K_1 = K_2 = K_3 = K$. Then (9) and (10) reduce to

$$K\frac{d^2\phi}{d\xi^2} - (e_1 - e_3)E_0 s\frac{d\theta}{d\xi} + \frac{(e_1 + e_3)\Delta\sigma}{\sigma_c}E_0 sc^2\frac{d\theta}{d\xi} = 0, \tag{13}$$

$$K\frac{d^2\theta}{d\xi^2} + \left[(e_1 - e_3) + \frac{\alpha_2}{\eta_1}(e_1 + e_3)c^2\right]E_0 s\frac{d\phi}{d\xi} - \frac{\alpha_2}{\eta_1}\frac{\varepsilon}{4\pi}\frac{\Delta\sigma}{\sigma_c}E_0^2 c^2\theta = 0. \tag{14}$$
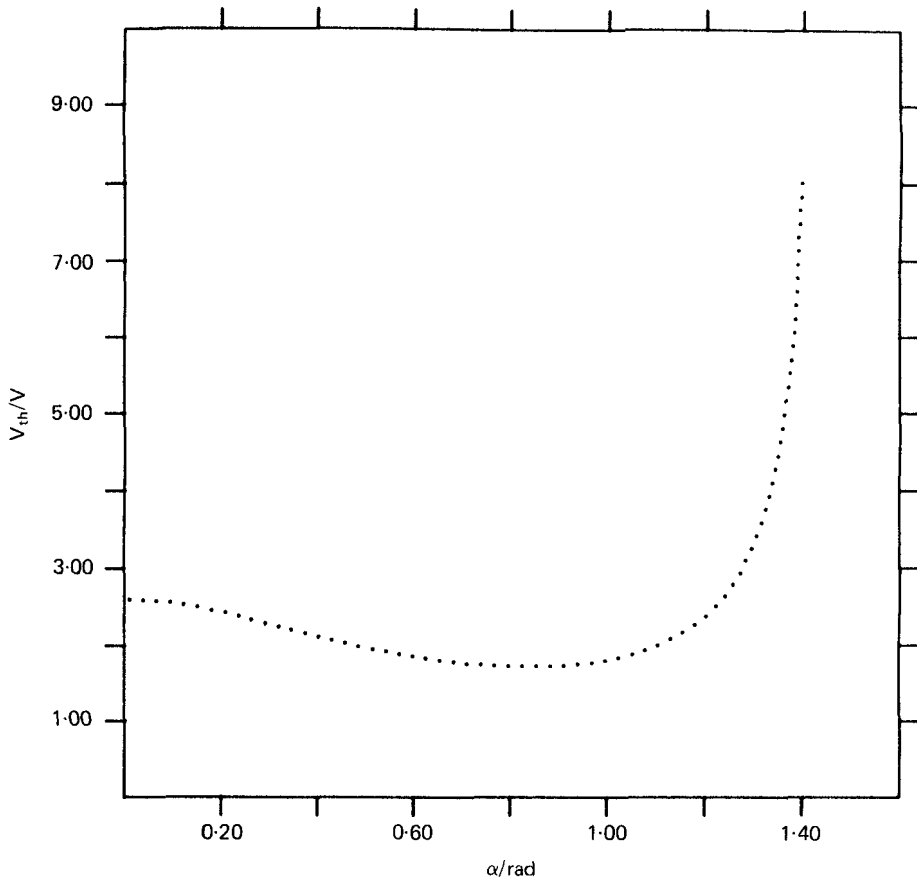
Figure 2. Variation of D.C. threshold voltage V_{th} with α calculated for the standard values of the MBBA parameters listed in the table.

Note that only the combinations $e_1 - e_3$ and $e_1 + e_3$ of the flexoelectric coefficients appear in these equations. The $e_1 - e_3$ terms in the two equations give the torque arising from the action of the external electric field on the curvature of the director field. The $e_1 + e_3$ term in (13) is the torque due to the gradient of the transverse electric field, and the $e_1 + e_3$ term in (14) is the hydrodynamic torque due to the action of the external field on the space-charge density arising from the flexoelectric polarization. If $e_1 - e_3$ and $e_1 + e_3$ have opposite signs then the two flexoelectric terms in (13) assist each other and favour a ϕ distortion. Let us choose $e_1 - e_3$ and $e_1 + e_3$ to be positive and negative respectively, as is found experimentally in MBBA. Taking θ_0, E_0 and α to be positive, we find from (13) that ϕ_0 is negative. Since α_2 is generally negative, both of the flexoelectric terms in (14) have the same sign. Further, the flexoelectric torques will be destabilizing if ϕ_0 is negative: at the threshold of the instability a ϕ distortion of the director and hence a non-zero value of α are favoured. Similar arguments apply when the signs of both θ_0 and ϕ_0 are reversed.

The dependence of α on $e_1 - e_3$ is shown in figure 3. As $e_1 - e_3$ is decreased from its initial positive value, the flexoelectric torques decrease and α decreases. As α becomes smaller, the hydrodynamic torque becomes more dominant and the decrease in α becomes very rapid. When $e_1 - e_3$ is negative and approximately equal to
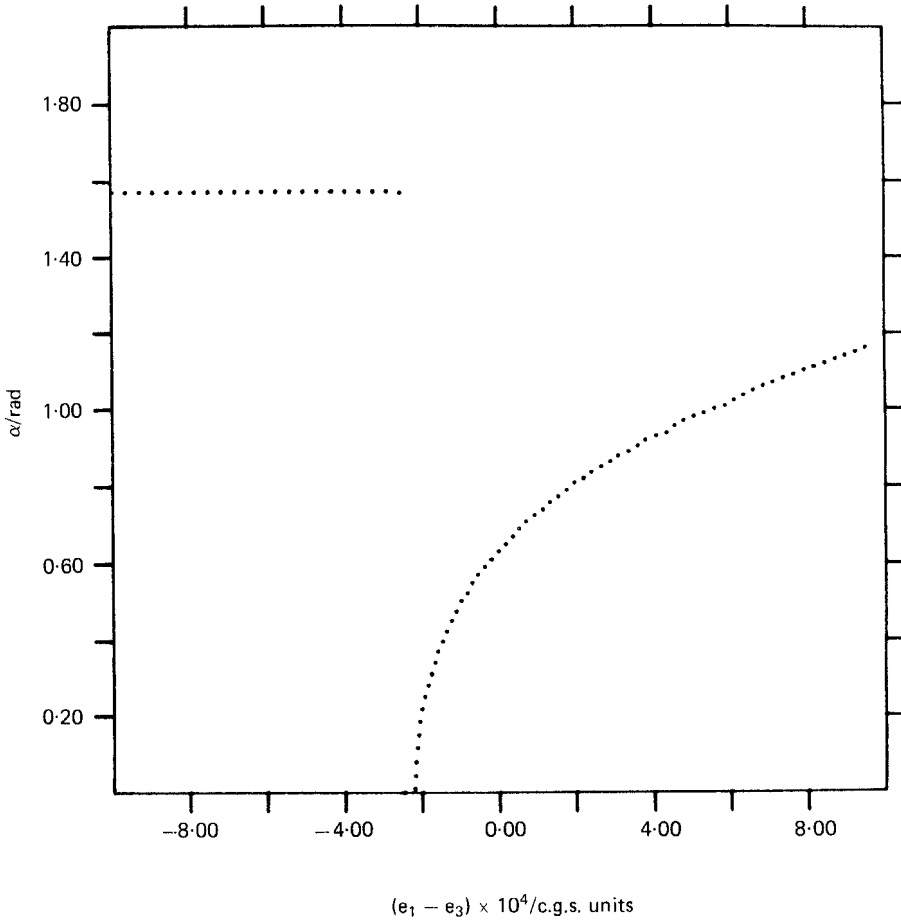
Figure 3.   Variation of α with $e_1 - e_3$ calculated for $\Delta\varepsilon = 0$ and $K_3 = K_2 = K_1$. Note that $\alpha = 0$ for a very small range of negative values of $e_1 - e_3$, and below this range the longitudinal flexoelectric domains are obtained.

$(\Delta\sigma/\sigma_\parallel)(e_1 + e_3)$ the net effect of the flexoelectric terms in (13) becomes negligible and α goes to zero. As $e_1 - e_3$ is decreased further, the threshold for the static flexoelectric domains [12] becomes smaller than that for the EHD instability when

$$|e_1 - e_3| > \left(\frac{-2\alpha_2 \varepsilon K}{\alpha_4 + \alpha_5 - \alpha_2} \frac{\Delta\sigma}{\sigma_\parallel} \right)^{1/2}$$

and $\alpha = \frac{1}{2}\pi$. Thus for a small range of values of $e_1 - e_3$ (see figure 3) the flexoelectric terms do not influence the problem, and $\alpha = 0$. The variation of α with $e_1 + e_3$ is shown in figure 4. As $e_1 + e_3$ is increased from its initial negative value, the flexoelectric torques decrease, and hence α decreases. When $e_1 + e_3$ is positive and in the range

$$\frac{-(\alpha_4 + \alpha_5 - \alpha_2)}{2\alpha_2}(e_1 - e_3) < e_1 + e_3 < \frac{\sigma_\parallel}{\Delta\sigma}(e_1 - e_3),$$

(13) and (14) cannot be satisfied by non-zero values of ϕ. As can be seen from figure 4, actually $\alpha = 0$ over a wider range because of the dominance of the hydro-dynamic torque at small values of α.
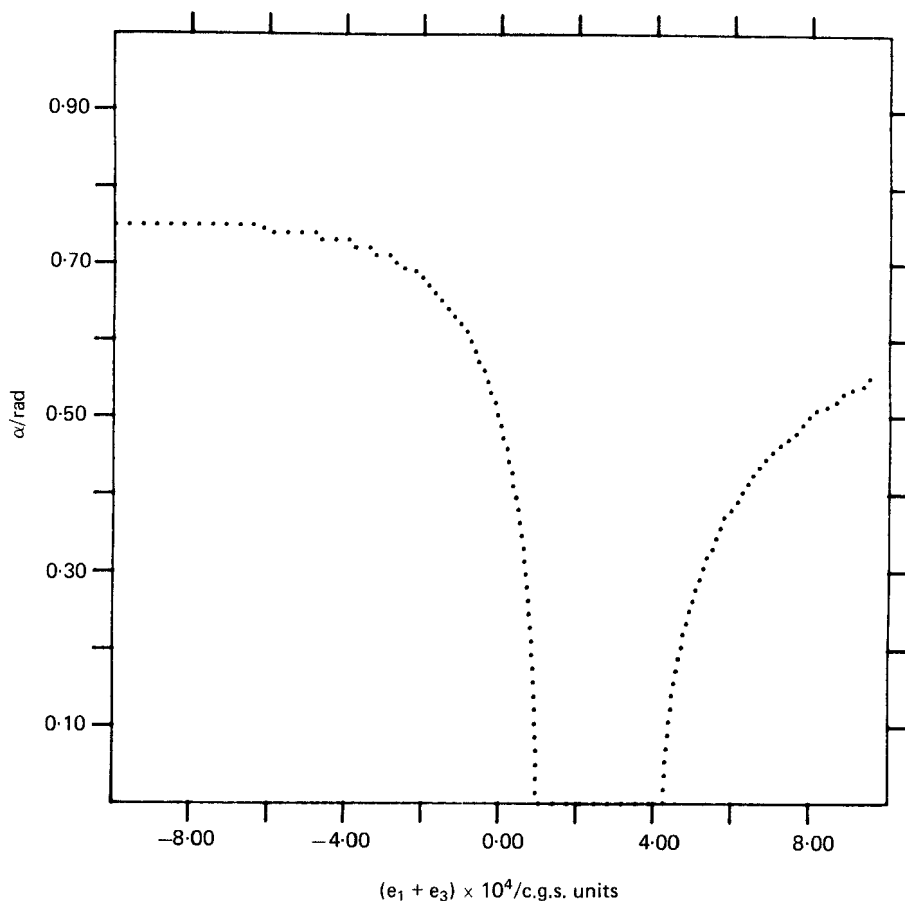
Figure 4. Variation of α with $e_1 + e_3$ calculated for $\Delta\varepsilon = 0$ and $K_3 = K_2 = K_1$. Note that $\alpha = 0$ for a small range of positive values of $e_1 + e_3$.

If we now introduce the elastic anisotropy, (9) and (10) show that, since K_2 and K_1 are less than K_3 in MBBA, the elastic anisotropy favours a non-zero value of α. This is reflected in figures 5 and 6, which show the variations of α with $e_1 - e_3$ and $e_1 + e_3$ respectively, for $K_1 \neq K_2 \neq K_3$ and $\Delta\varepsilon = 0$.

The variations of V_c and α with $\Delta\varepsilon$ are shown in figures 7 and 8 respectively. As $\Delta\varepsilon$ is increased, the stabilizing torque on the director decreases and V_c decreases. It should be noted that, beyond a certain positive value of $\Delta\varepsilon$, the Freedericksz transition has a lower threshold than the E.H.D. instability. When $\Delta\varepsilon$ is negative the space-charge density due to the dielectric polarization has the same sign as that due to the conductivity anisotropy. Therefore, on increasing α from its initial negative value, the total space-charge density and hence the hydrodynamic torque decrease (see (10)). The latter equation can, however, be satisfied by an increase in the value of α due to the flexoelectric terms (figure 8).

It is interesting to note that if both the flexoelectric coefficients are decreased by a factor S, fixing the ratio of $(e_1 - e_3)/(e_1 + e_3)$ at the MBBA value, then a non-zero value of α is obtained only if $S > 0.13$ (figure 9).

Figures 10 and 11 show V_c and α as functions of $\Delta\sigma/\sigma_\perp$. When the latter has a small value, the Carr–Helfrich mechanism is not very efficient and the flexoelectric terms
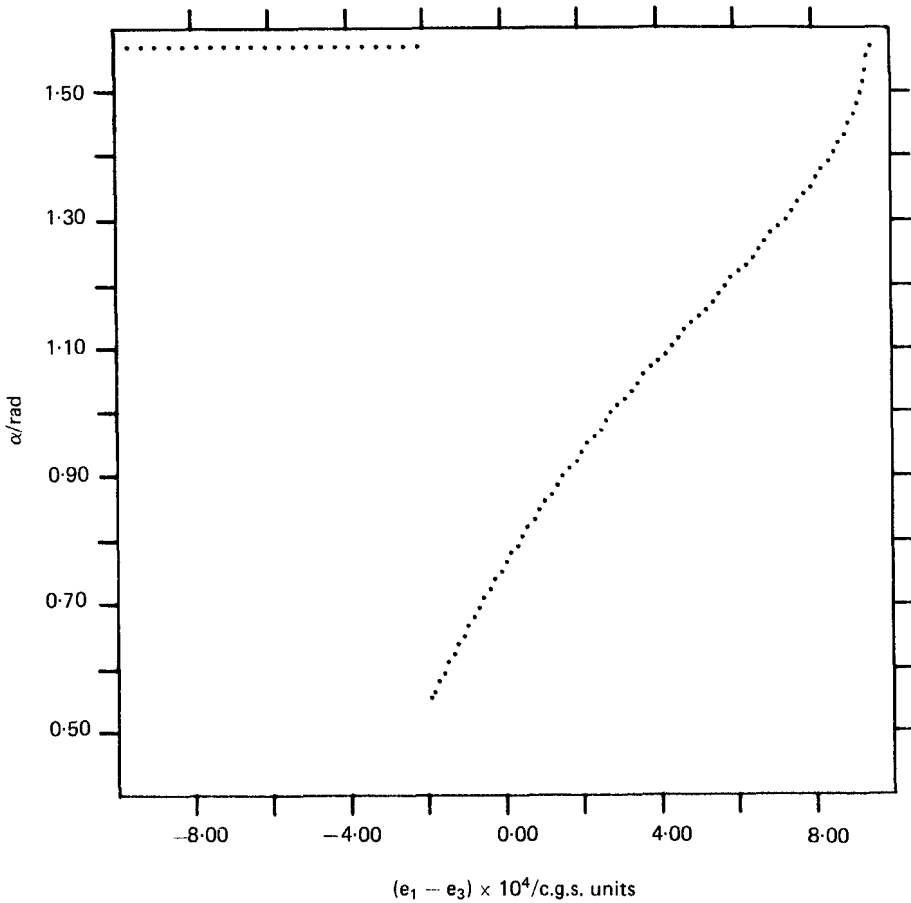
Figure 5.   Variation of α with $e_1 - e_3$ calculated for $\Delta\varepsilon = 0$ and including the elastic anisotropy. Note that α does not go to zero in this case.

dominate, and hence α and V_c are large. As $\Delta\sigma/\sigma_\perp$ is increased, the Carr–Helfrich mechanism becomes more efficient and both V_c and α decrease initially. With further increase in $\Delta\sigma/\sigma_\perp$, V_c continues to decrease while α gradually increases. The increase in $\Delta\sigma/\sigma_\perp$ increases the transverse electric field gradient (see (5)) and hence the flexoelectric torque on the director as well as the value of α.

3.1. *Experimental results*

Most of the D.C. studies on E.H.D. instabilities in nematics have been made on MBBA. This material is chemically unstable, and the D.C. instability exhibited by it is known to be influenced by charge injection at the electrodes [5]. Consequently the optical pattern observed at the onset of the instability is not the set of linear rolls expected from the Carr–Helfrich mechanism, but rather a complicated two-dimensional pattern [5, 13]. We have studied a room-temperature nematic mixture containing two chemically stable compounds, namely CE-1700 and PCH-302 from Roche Chemicals. The low-frequency principal dielectric constants and the principal conductivities were measured at 1592 Hz using a Wayne Kerr (B642) bridge. The
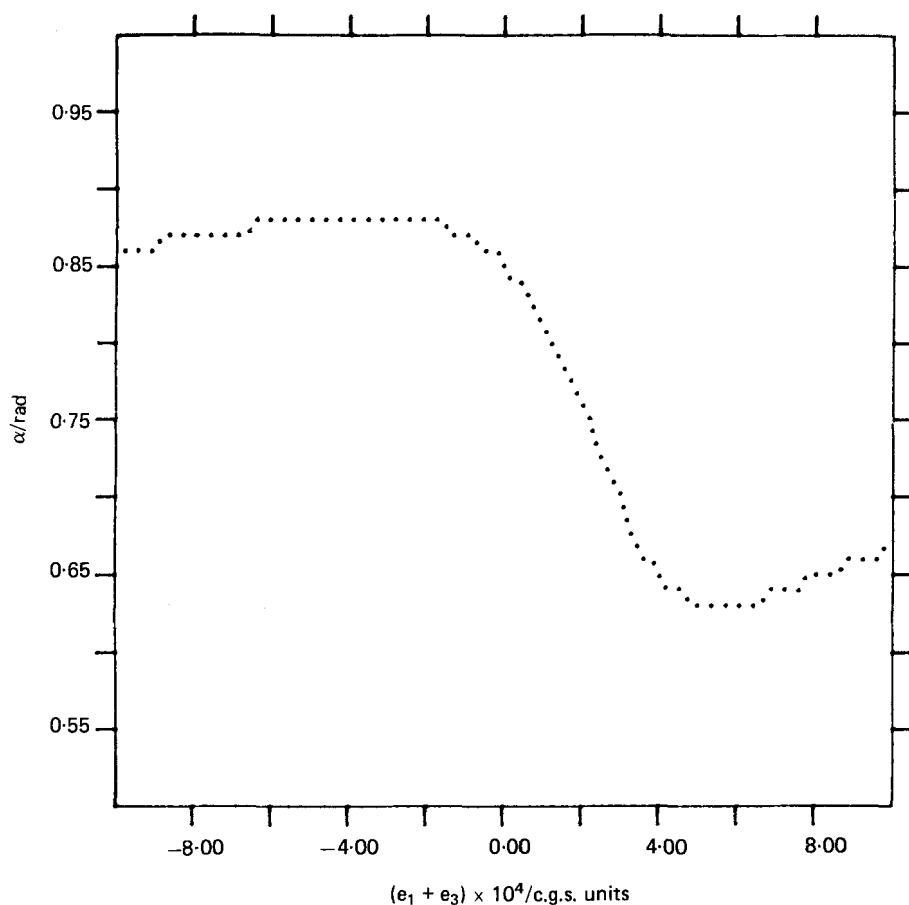
Figure 6. Variation of α with $e_1 + e_3$ calculated for $\Delta\varepsilon = 0$ and including the elastic anisotropy. In this and some of the other figures the coarseness in the plot is due to a relatively low resolution on the monitor from which a hard copy was obtained.

values obtained at room temperature are: $\varepsilon_{\parallel} = 3\cdot3$, $\varepsilon_{\perp} = 4\cdot3$ and $\sigma_{\parallel}/\sigma_{\perp} = 1\cdot1$. As our main objective was to study the influence of flexoelectricity on the D.C. E.H.D. instability, we also measured the flexoelectric coefficients of this mixture. The experimental details are described elsewhere [14]. $(e_1 - e_3)/K$ and $(e_1 + e_3)/K$ were found to be 100 and -180 c.g.s. units respectively. Note that these values are comparable to the MBBA values (see the table) and have the same signs.

The sample thickness was typically about $20\,\mu m$ in most of the studies. Under D.C. excitation the E.H.D. instability sets in as a set of convective rolls (figure 12). Further, the instability was not observed when the thickness of the sample was less than about $5\,\mu m$. As is well known [2], the existence of a critical thickness below which the E.H.D. instability cannot be observed is characteristic of the Carr–Helfrich mechanism, where the space charges are formed owing to the anisotropy of the electrical conductivity in the presence of a bend distortion of the director field. As the thickness of the sample is decreased, the director relaxation time decreases, becoming smaller than the charge relaxation time when the thickness is less than a critical value. Hence the fluctuations in the director field do not last long enough for the formation
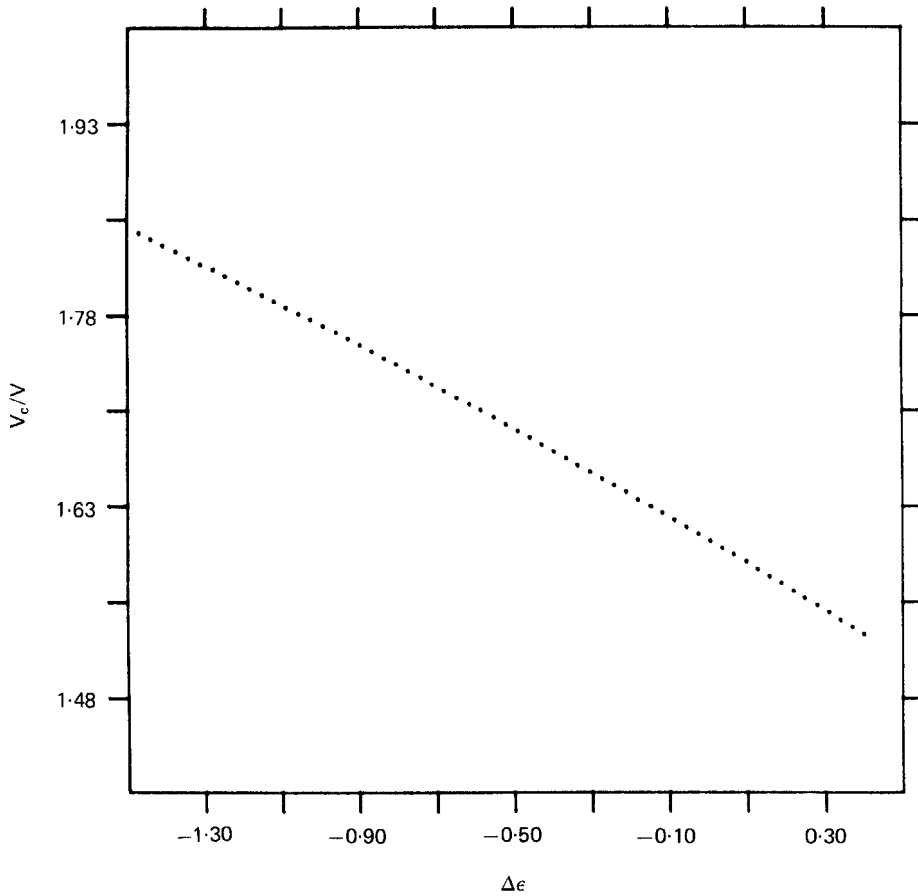
Figure 7.   Variation of the critical voltage V_c with the dielectric anisotropy $\Delta\varepsilon$.

of space charges. Further, as can be seen from (2) and (3), the flexoelectric polarization makes an additional contribution to the space-charge density. The above argument concerning a critical thickness remains valid for charges arising from both mechanisms. We conclude that these mechanisms are responsible for the D.C. instability in our nematic mixture, which is observed only above a critical thickness, and that the influence of charge injection is negligible. The instability was found to set in at a threshold voltage of about 8·5 V, with the wave vector of the convective rolls making an angle of about 20° with the direction of initial alignment of the director. Although the occurrence of these oblique rolls is clearly predicted by the theory presented above, a detailed comparison of the theoretical predictions with the experimental results is not possible since many of the material parameters of the mixture under study are unknown.

We also found that the width of the optical domains is approximately twice the sample thickness. Dust-particle motion within these domains clearly shows that each optical domain consists of two convective rolls of opposite vorticity. This is also indicated by the observation that an edge dislocation in the optical pattern corresponds to the termination of just one optical domain (figure 12).
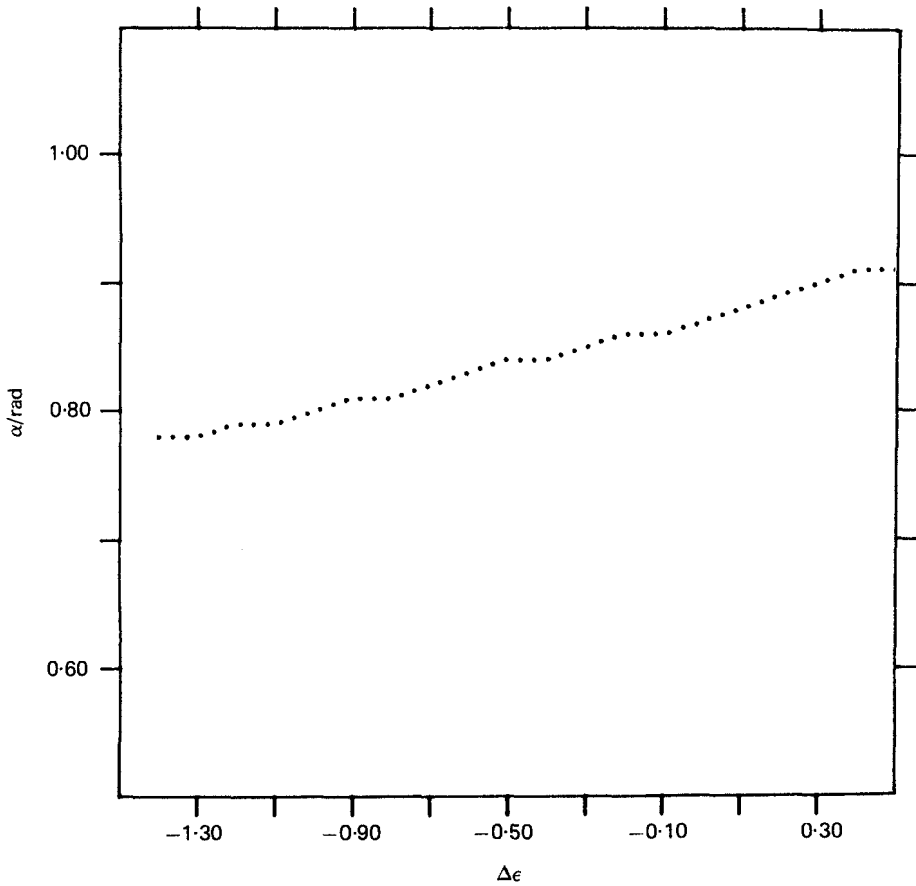
Figure 8. Variation of α with the dielectric anisotropy $\Delta\varepsilon$.

Figure 13 shows the dark fringes obtained when the sample, placed between crossed polarizers, is viewed through a tilting compensator. These dark bands correspond to regions where the phase difference introduced by the sample in the incident linearly polarized beam is offset by the compensator. These fringes show very clearly that the effective birefringence of the sample varies more sharply at the bright lines of figure 12 than in the region midway between two bright lines. When the field is increased beyond the threshold, this asymmetry in the variation of the effective birefringence in these two regions becomes more pronounced (figure 13 (*b*)). These observations indicate that the director profile within the rolls is non-sinusoidal, with the curvature in the region of the bright lines being much stronger than that in the region midway between two bright lines. The increase in the asymmetry with field strength above the threshold shows that non-linear terms are responsible for the observed optical pattern. Further, when the field direction is reversed, the bright lines making up the optical pattern are found to shift by about half the optical-domain width. The polarity dependence of the optical pattern suggests that flexoelectricity may be responsible for the non-sinusoidal director profile, since it is the only bulk property of a nematic that couples linearly to an external electric field. Including the second-order terms and taking $\alpha = 0$ for simplicity, the torque balance equation
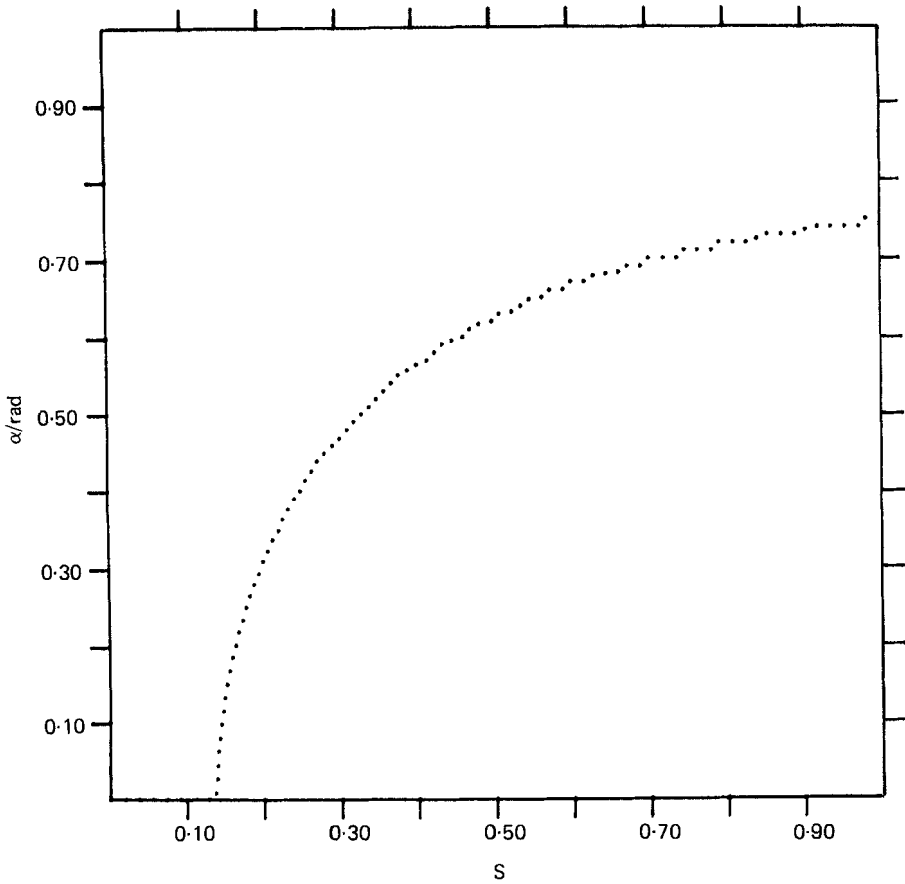
Figure 9.   Variation of α with the factor S by which the flexoelectric coefficients are decreased.

along Y is given by

$$K_3 \frac{d^2\theta}{dX^2} + \left[\frac{\Delta\varepsilon}{4\pi} \frac{\sigma_\perp}{\sigma_\parallel} + \frac{\alpha_2}{\eta} \frac{\varepsilon_\parallel}{4\pi} \left(\frac{\Delta\varepsilon}{\varepsilon_\parallel} - \frac{\Delta\sigma}{\sigma_\parallel} \right) \right] E_0^2 \theta - (e_1 + e_3) \frac{\alpha_2}{\eta_1} E_0 \theta \frac{d\theta}{dX} = 0,$$

$$(15)$$

where $\eta = \frac{1}{2}(\alpha_4 + \alpha_5 - \alpha_2)$. The lone quadratic term in the above equation arises from the action of E_0 on the flexoelectric contribution to the space-charge density. This equation was solved graphically by the phase-plane technique, using the MBBA values of the material parameters. The resulting non-sinusoidal θ profile and the effective birefringence Δn are shown in figure 14. The variation of Δn is sharper in regions like B than in regions like A. The incident light is therefore brought to focus at two different planes by the two types of regions. When the microscope is focused on the set of bright lines due to regions like B, which is closer to the sample, the lines corresponding to regions like A become very diffuse and faint. The disposition of the convective rolls with respect to the bright lines shown in figure 14 agrees with the observed dust-particle motion. When the field is reversed, the director field in regions
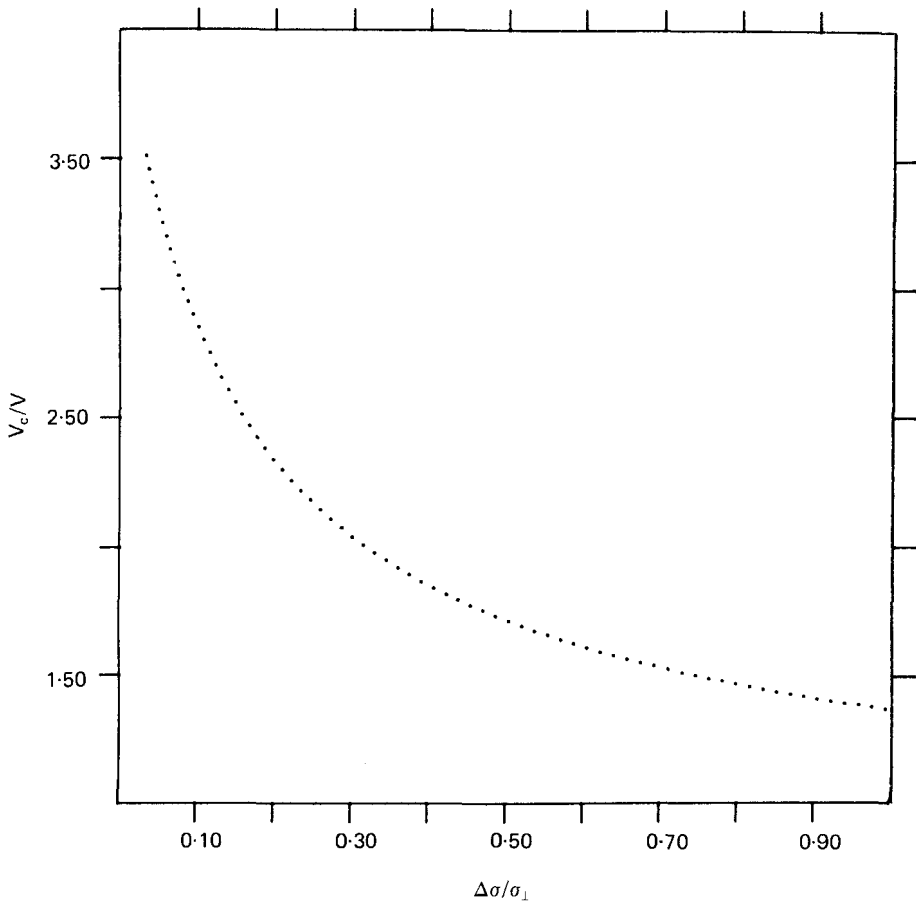
Figure 10. Variation of the critical voltage V_c with $\Delta\sigma/\sigma_\perp$.

like A becomes more distorted than in regions like B, and the bright lines shift to A in agreement with the observations.

We should note here that, as discussed by Hirata and Tako [15], an asymmetry in the optical pattern will also arise from a sinusoidal director profile in the convective rolls. This is caused by tilting of the rays due to the periodic variation of the effective extraordinary refractive index in the sample. However, this weaker asymmetry does not depend on the polarity of the applied field, since the director profile in the conduction regime does not change with the sign of the field, and is also present with an applied A.C. field.

Our experiments also indicate that the fluid particles move along helical trajectories within the rolls. A three-dimensional model developed by us [9] that takes into account the boundary conditions shows that the flexoelectric effect is entirely responsible for the helical flow. When the flexoelectric terms are neglected, this model is in agreement with that developed by Zimmermann and Kramer [16] using stress-free boundary conditions. More recently the latter authors have also reported calculations taking flexoelectric terms into account [17].
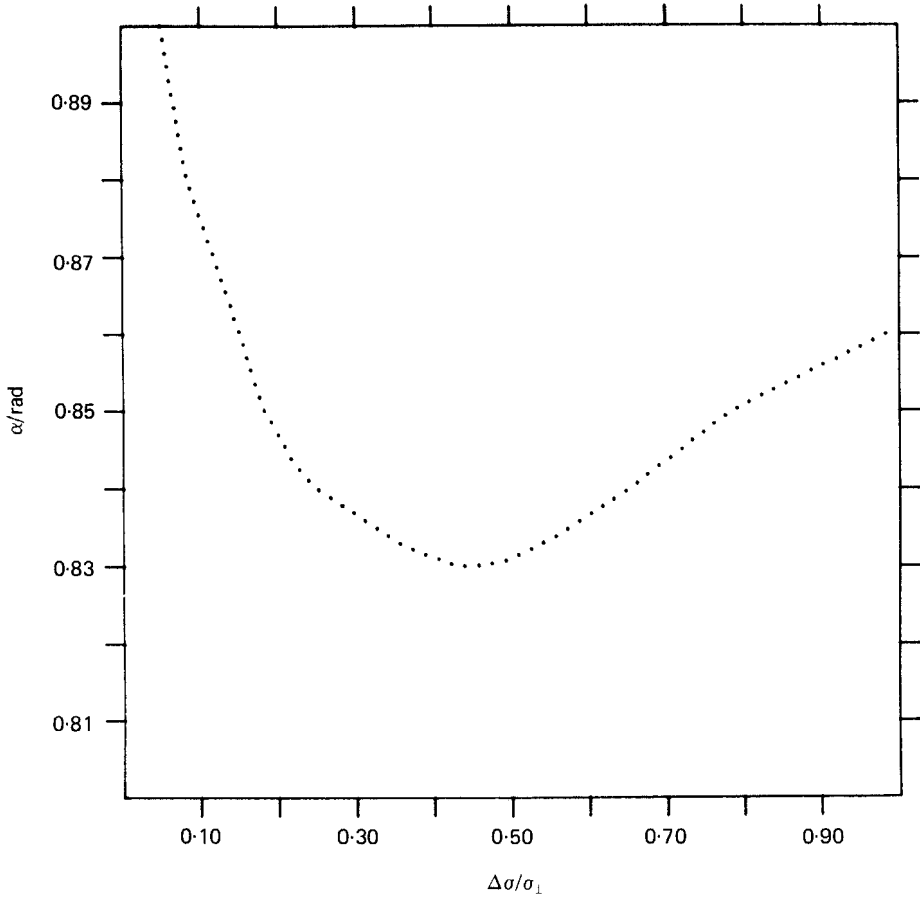
Figure 11.   Variation of α with $\Delta\sigma/\sigma_\perp$.

4. A.C. excitation

Eliminating v_z and E_ξ from (4)–(8) and assuming the solutions

$$\psi = \psi(t) \exp (iq\xi),$$

$$\phi = \phi(t) \exp (iq\xi),$$

$$Q = Q(t) \exp (iq\xi),$$

where $\psi = \partial\theta/\partial\xi$, the following equations are obtained describing the response of the system to an external electric field:

$$\dot\psi + \frac{\psi}{T_\psi} + \frac{\varrho_1 E_0}{\eta_2} \phi + \frac{AE_0}{\eta_2} Q = 0, \tag{16}$$

$$\dot\phi + \frac{\phi}{T_\phi} + \frac{e_\psi E_0}{\gamma_1} \psi + \frac{e_\varrho}{\gamma_1} Q = 0, \tag{17}$$

$$\dot Q + \frac{Q}{\tau} + \sigma_\psi E_0 \psi + \frac{\varrho_2}{\tau} \phi = 0, \tag{18}$$
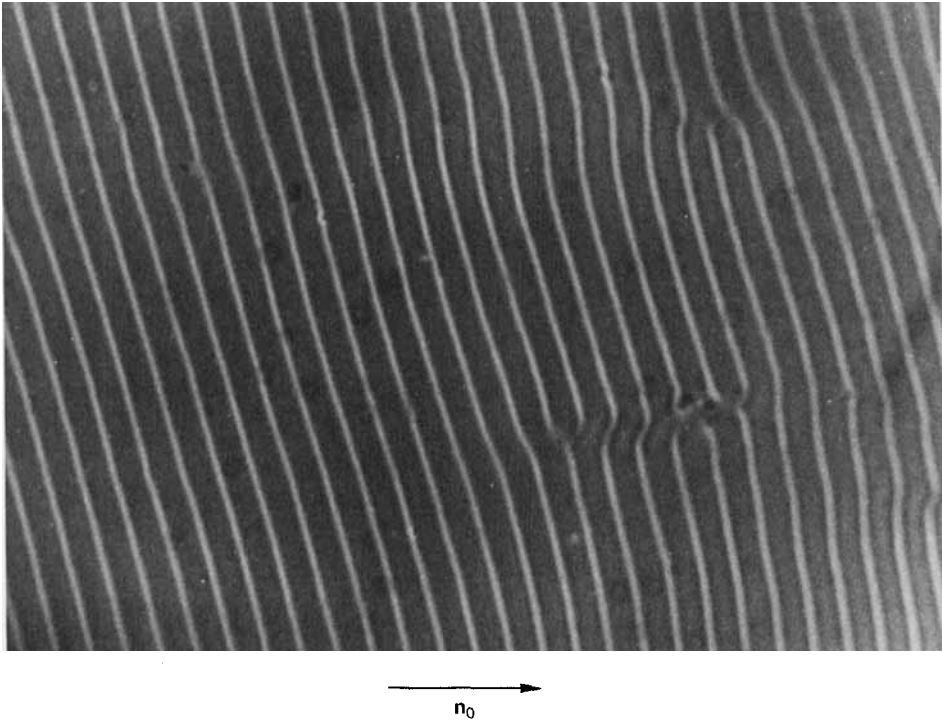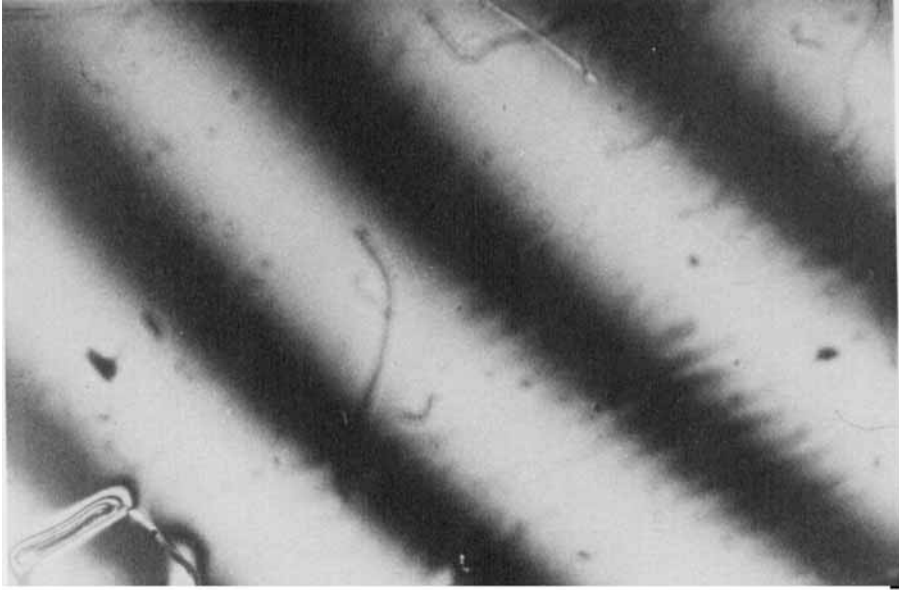
$$\xrightarrow{\quad\quad\quad\quad} \quad n_0$$

Figure 12. Photograph of the E.H.D. pattern observed slightly above the threshold of the D.C. instability in a room-temperature nematic. The orientation of the undistorted director n_0 is indicated in the figure. Note that the edge dislocation in the pattern corresponds to the addition of one optical domain, which has two convective rolls of opposite vorticity as explained in the text. The sample thickness was about 15 μm. ($\times$ 300)

where

$$\frac{1}{T_\psi} = \left(Mq^2 - \frac{\varepsilon_\perp \varepsilon_R E_0^2}{4\pi}\right)\bigg/\eta_2,$$

$$\varrho_1 = [e_1 - e_3 - (e_1 + e_3)c^2 \varepsilon_R]sq^2,$$

$$A = -\left(\frac{\alpha_2}{\eta_1} + \varepsilon_R\right)c, \qquad \eta_2 = \alpha_3 - \alpha_2 - \frac{\alpha_2^2 c^2}{\eta_1},$$

$$\frac{1}{T_\phi} = \left[L + \frac{4\pi(e_1 + e_3)^2 s^2 c^2}{\varepsilon_c}\right]\frac{q^2}{\alpha_3 - \alpha_2},$$

$$e_\varrho = \frac{4\pi(e_1 + e_3)cs}{\varepsilon_c},$$

$$e_\psi = (e_1 - e_3)s - \frac{\Delta\varepsilon\, ce_\varrho}{4\pi},$$

$$\frac{1}{\tau} = \frac{4\pi\sigma_c}{\varepsilon_c}, \qquad \sigma_\psi = (\Delta\sigma - \sigma_c \varepsilon_R)c,$$

$$\varrho_2 = (e_1 + e_3)csq^2.$$

(a)
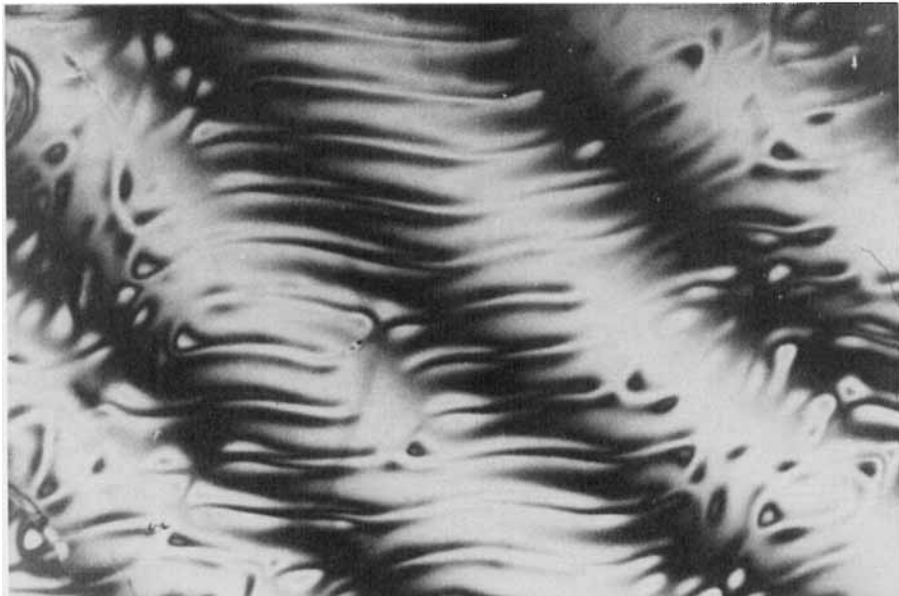
(b)

Figure 13.   (a) Dark fringes obtained when the sample was viewed in sodium light through a tilting compensator. The applied voltage was close to the threshold value. (b) As in (a), but at a slightly higher voltage.

For the sake of simplicity, following Smith *et al.* [3], we solve the problem for the case of square-wave excitation. The applied field is now given by

$$E_0(t) = \begin{cases} + E_0 & (0 < t < (2v)^{-1}), \\ - E_0 & ((2v)^{-1} < t < v^{-1}), \end{cases}$$
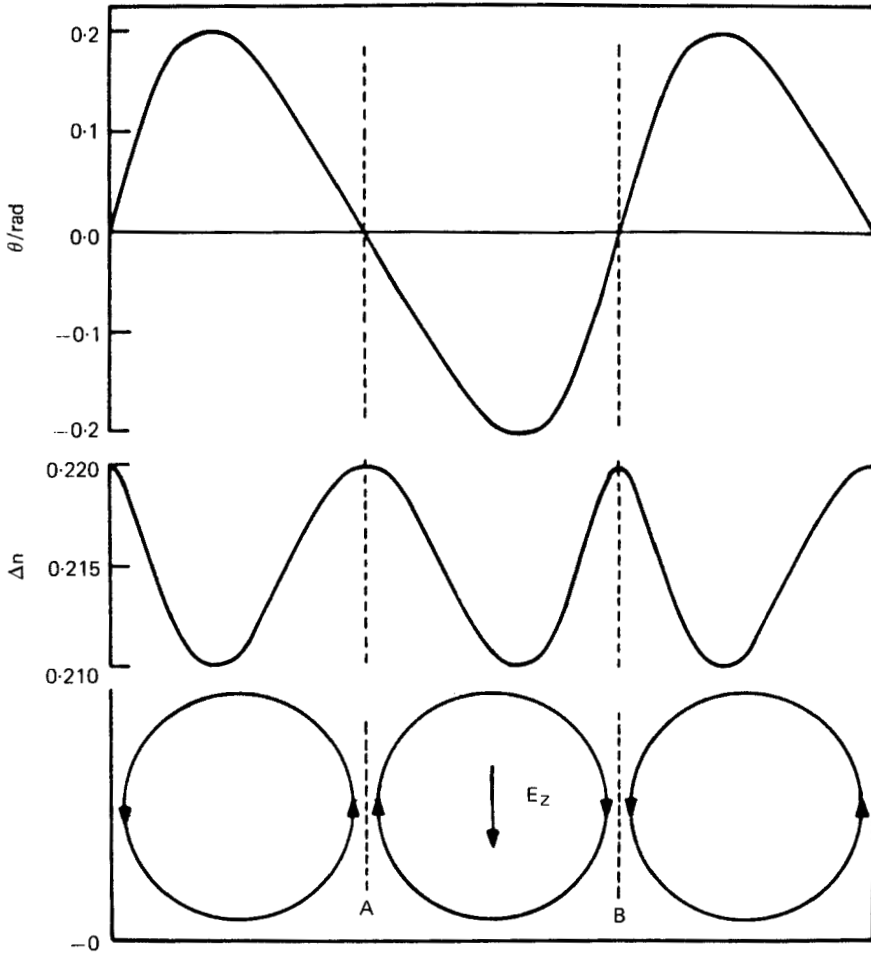
Figure 14. Top: non-sinusoidal director profile obtained from (15). Centre: resulting variation of the effective birefringence Δn with X (for $n_e = 1 \cdot 769$, $n_0 = 1 \cdot 549$). Bottom: the disposition of the convective rolls agrees with the observed dust-particle motion, the regions B corresponding to the bright lines of figure 12.

v being the frequency of the applied A.C. field. Taking solutions of the form

$$\psi(t) = C_\psi \exp(\lambda t/\tau),$$
$$\phi(t) = C_\phi \exp(\lambda t/\tau),$$
$$Q(t) = C_Q \exp(\lambda t/\tau),$$

for one half-period of the applied field, the following characteristic equation is obtained:

$$\lambda^3 \frac{1}{\tau^3} + \lambda^2 \left(\frac{1}{\tau^3} + \frac{1}{\tau^2 T_\phi} + \frac{1}{\tau^2 T_\psi} \right)$$
$$+ \lambda \left(\frac{1}{\tau^2 T_\phi} - \frac{e_\varrho \varrho_2}{\gamma_1 \tau^2} + \frac{1}{\tau^2 T_\psi} + \frac{1}{\tau T_\psi T_\phi} - \frac{e_\psi \varrho_1 E_0^2}{\eta_2 \gamma_1 \tau} - \frac{A\sigma_\psi E_0^2}{\eta_2 \tau} \right)$$
$$+ \frac{1}{\tau T_\psi T_\phi} - \frac{e_\varrho \varrho_2}{\gamma_1 \tau T_\psi} - \frac{\varrho_1 e_\psi E_0^2}{\eta_2 \gamma_1 \tau} + \frac{\varrho_1 \sigma_\psi e_\varrho E_0^2}{\eta_2 \gamma_1} - \frac{A\sigma_\psi E_0^2}{\eta_2 T_\phi} + \frac{Ae_\psi \varrho_2 E_0^2}{\eta_2 \gamma_1 \tau} = 0. \quad (19)$$

The general solutions are of the form

$$\psi(t) = \sum_{j=1}^{3} a_j \exp\left(\frac{\lambda_j t}{\tau}\right),$$

$$\phi(t) = \sum_{j=1}^{3} b_j \exp\left(\frac{\lambda_j t}{\tau}\right),$$

$$Q(t) = \sum_{j=1}^{3} c_j \exp\left(\frac{\lambda_j t}{\tau}\right),$$

where a_j are arbitrary constants, λ_j are the eigenvalues of (19), and

$$b_j = \frac{T_\phi[\tau T_\psi A e_\psi E_0^2 - \eta_2 e_\varrho(\lambda_j T_\psi + \tau)]}{T_\psi[\tau T_\phi e_\varrho \varrho_1 E_0 - \gamma_1 A E_0(\lambda_j T_\phi + \tau)]} a_j,$$

$$c_j = \frac{\eta_2 \gamma_1 (\lambda_j T_\phi + \tau)(\lambda_j T_\psi + \tau) - \tau^2 T_\psi T_\phi \varrho_1 e_\psi E_0^2}{\tau T_\psi[\tau T_\phi e_\varrho \varrho_1 E_0 - \gamma_1 A E_0(\lambda_j T_\phi + \tau)]} a_j.$$

It is clear from (16)–(18) that when E_0 changes sign after every half period, either ϕ and Q change sign or ψ changes sign. Thus there are two sets of solutions possible, corresponding to different physical situations, as in the Orsay model [2, 3]:

(a) *the conduction regime*: here Q and ϕ oscillate with the field but ψ does not, i.e.

$$\left.\begin{array}{l} Q(t + 1/2\nu) = -Q(t), \\ \phi(t + 1/2\nu) = -\phi(t), \\ \psi(t + 1/2\nu) = \psi(t); \end{array}\right\} \qquad (20)$$

(b) *the dielectric regime*: here ψ oscillates with the field but Q and ϕ do not, i.e.

$$\left.\begin{array}{l} \psi(t + 1/2\nu) = -\psi(t), \\ Q(t + 1/2\nu) = Q(t), \\ \phi(t + 1/2\nu) = \phi(t). \end{array}\right\} \qquad (21)$$

In order to find the threshold of instability, a set of eigenvalues λ_1, λ_2 and λ_3 of (19) must be found that satisfy either (20) or (21). The problem was solved numerically. For a given set of values of the material parameters and a given frequency, we choose some values of α and the voltage V and obtain the eigenvalues of (19). The voltage V is then varied till the λs satisfy one of the two conditions corresponding to the two regimes of instability. This value of V is the threshold voltage V_{th} for the particular value of α chosen. The calculations are repeated for different values of α. The minimum value of V_{th} gives the critical voltage V_c for the onset of instability, and the corresponding value of α is the angle between $\mathbf{q}$ and $\mathbf{n}_0$ at the onset of instability. The calculations are then repeated for different values of the frequency of the applied field.

The variation of the critical voltage V_c and the corresponding value of α with frequency are shown in figure 15 for the MBBA parameters (see the table) with $\sigma_\| = 3 \times 10^{-10}$ ohm^{-1} cm^{-1}. Curves (a) and (c) correspond respectively to the conduction and dielectric regimes. Curve (b) is the re-stabilization branch, above which the conduction regime cannot exist. The dashed lines in the stability diagram indicate regions with a non-zero value of α. We see from the figure that oblique rolls are obtained up to a critical frequency ν_0 in the conduction regime, as found
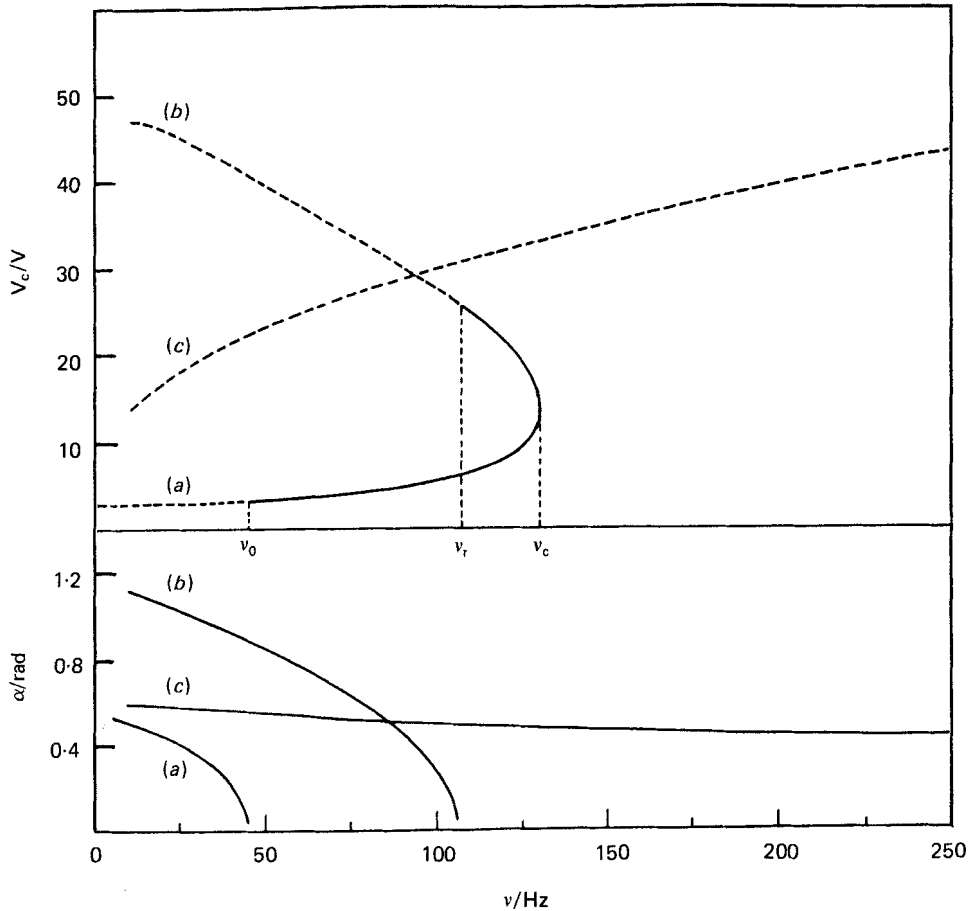
Figure 15. Upper section: Threshold voltage (curve (*a*)) and restabilization voltage (curve (*b*)) as functions of the frequency in the conduction regime for MBBA with $\sigma_\parallel = 3 \times 10^{-10}\,\text{ohm}^{-1}\,\text{cm}^{-1}$. The low-frequency portions indicated by dashed lines are characterized by non-zero values of α. The frequency dependence of the voltage at threshold for a 20 μm thick sample in the dielectric regime is shown by curve (*c*). Lower section: Variations of tilt angle α of the oblique rolls with frequency. (*a*), (*b*) and (*c*) correspond to the respective branches in the upper section.

experimentally by Ribotta *et al.* [4]. Further, the ratio v_0/v_c, where v_c is the cut-off frequency of the conduction regime, is comparable to the experimental value [4].

Oblique rolls are also obtained along the restabilization branch up to a frequency v_r, with $v_0 < v_r < v_c$. Therefore, for frequencies in the range $v_0 < v < v_r$, although normal rolls are obtained at the threshold, we can expect oblique rolls as the field strength is raised. This is again in agreement with the observations of Ribotta *et al.* [4]. A non-linear analysis is needed to calculate the voltage at which this transition takes place.

In the dielectric regime a non-zero value of α is obtained at the threshold for all frequencies (see figure 15, curve (*c*)). Experimental observations in this regime are available only on MBBA [5]. In this case a set of normal rolls is seen at the threshold. We note here that if the flexoelectric coefficients are decreased by a factor S, keeping the ratio $(e_1 - e_3)/(e_1 + e_3)$ fixed, then a non-zero value of α is obtained only if
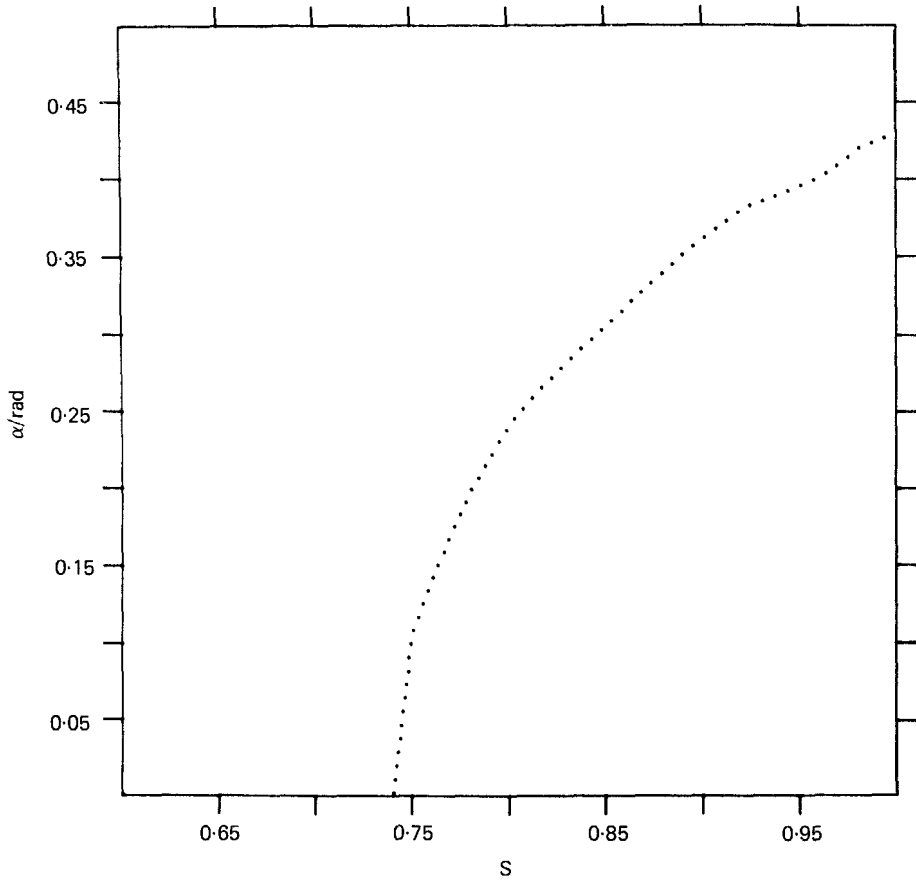
Figure 16.   Variation of α with the factor S by which the flexoelectric coefficients are decreased, at 100 Hz in the dielectric regime.

$S > 0.74$ (figure 16). It is possible that the experimental values of the flexoelectric coefficients of MBBA listed in the table may have been overestimated. We should note, however, that, with a very slight increase in the field above the threshold, the chevron pattern consisting of *oblique* rolls is observed in MBBA [5]. In view of our earlier discussion concerning the occurrence of oblique rolls above the threshold in the frequency range $v_0 < v < v_r$ in the conduction regime, we believe that flexoelectricity is again responsible for the oblique rolls found in the chevron pattern.

The relaxation time of the ϕ distortion, T_ϕ, is independent of the applied field (see (17)) and typically of the order of a few hertz. However, because of the coupling to the other two variables, ϕ is forced to oscillate with the applied field even at higher frequencies in the conduction regime. Figure 17 (a) shows ψ, Q and ϕ as functions of time for one period of the applied field at a voltage just above the threshold and at a frequency slightly less than v_0 in the conduction regime. The temporal behaviour of these three variables can be understood from (16)–(18). The ϕ terms in (16) and (18) are found to be negligible, and hence the evolutions of both ψ and Q are similar to those discussed by Smith *et al.* [3]. We shall therefore confine our attention to the evolution of ϕ. Let the field be reversed at $t = 0$ when ψ, ϕ and Q are positive and increasing. Of the two forcing terms in (17), only the one containing ψ changes sign
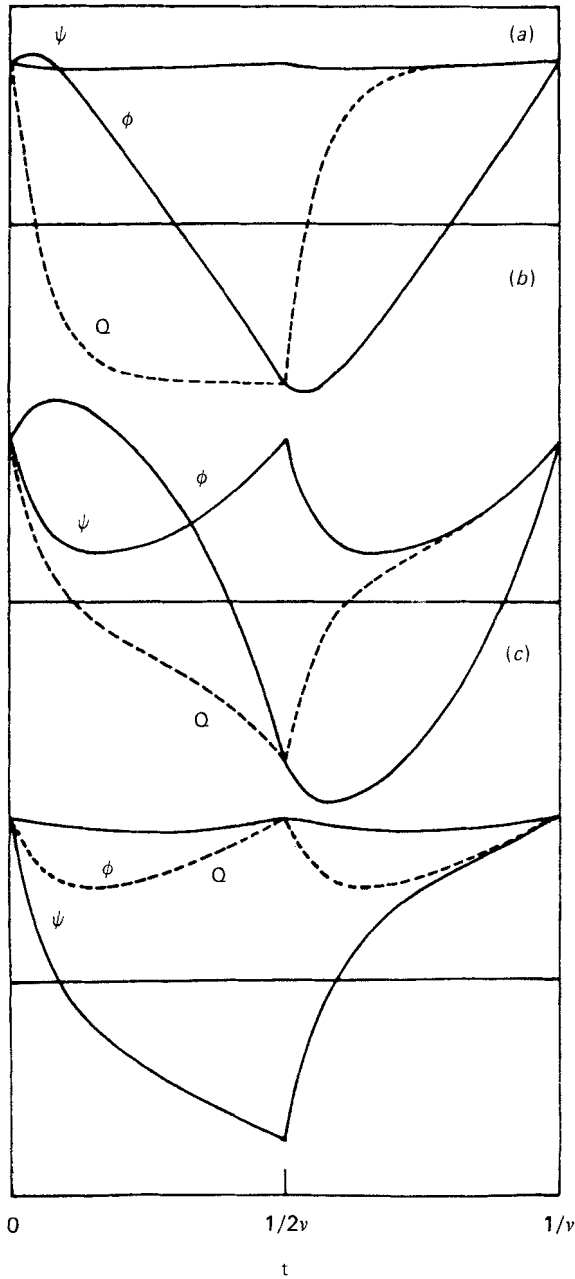
Figure 17. Variations of ψ, ϕ and Q with time for one period of the applied square-wave electric field: (a) just above the threshold in the conduction regime at 40 Hz; (b) slightly below the restabilization curve at 100 Hz; (c) in the dielectric regime at 170 Hz. The values of the material parameters used in these calculations are the same as in figure 15.

immediately, and ϕ continues to increase since the Q term is stronger than the ψ term. However, as soon as Q becomes negative, both forcing terms have the same sign and ϕ decreases and changes sign. Thus Q and ϕ oscillate with the applied field. Figure 17 (b) corresponds to a voltage slightly below the restabilization curve and at
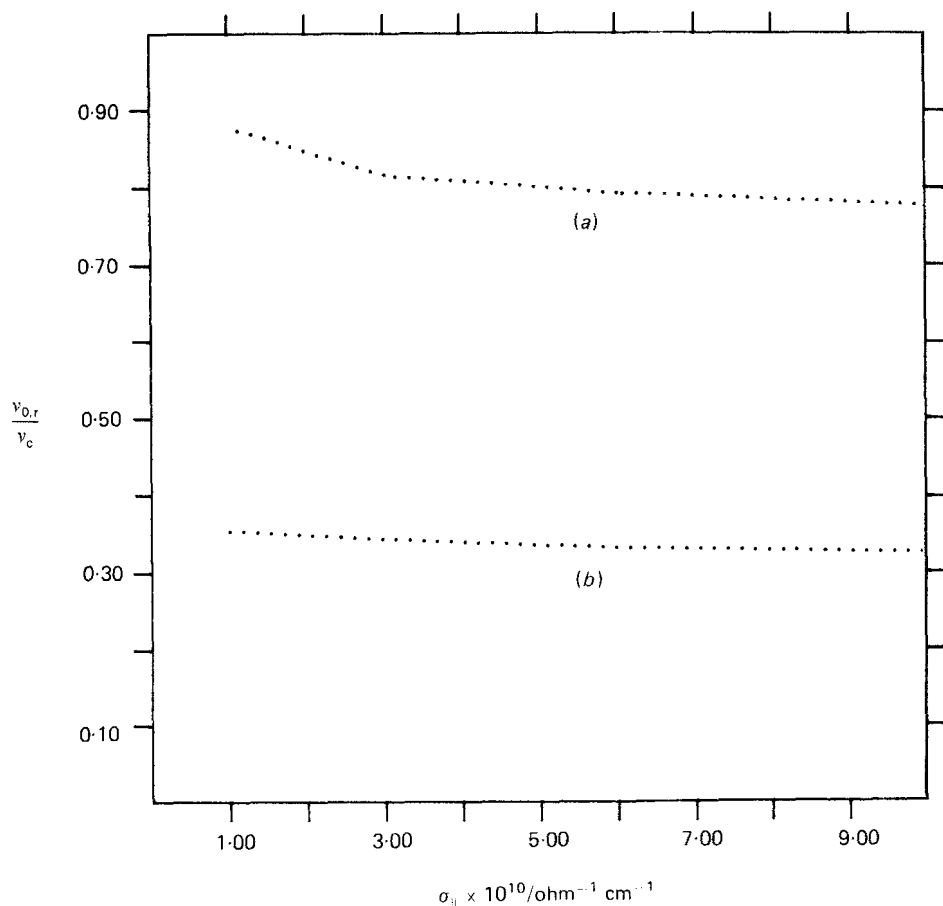
Figure 18.   Variation of the ratios of frequencies v_0/v_c (curve (a)) and v_r/v_c (curve (b)) with $\sigma_\parallel$.

a frequency slightly less than v_r. Since T_ψ is now comparable to τ, the initial decrease in ψ is very sharp. The evolution of ϕ is as in the previous case. The larger value of E along the restabilization branch makes the ψ term in (17) stronger, allowing ϕ to oscillate at higher frequencies than at the threshold of the conduction regime. As a result, oblique rolls are obtained along the restabilization branch up to a frequency $v_r > v_0$. In the dielectric regime ψ oscillates with the applied field, while Q and ϕ do not (figure 17(c)). In this regime a ϕ distortion of the director field can occur if the values of the material parameters are suitably chosen, irrespective of the frequency.

It is clear from the above discussion that ϕ is driven and made to oscillate in the conduction regime mainly by the Q term in (17). By increasing the conductivity of the sample, the charge relaxation time decreases and ϕ is forced to oscillate at higher frequencies. Figure 18 shows the variations of v_0/v_c (curve (a)) and v_r/v_c (curve (b)) with $\sigma_\parallel$ for fixed $\Delta\sigma/\sigma_\parallel$. As seen from the figure, both of these ratios decrease as $\sigma_\parallel$ is increased, with v_r/v_c decreasing more rapidly at smaller values of $\sigma_\parallel$.

In some materials that exhibit a smectic A (or C)–nematic transition the conductivity anisotropy $\Delta\sigma$ becomes negative as the temperature is lowered towards the transition point. Two regimes of E.H.D. instability are observed in these nematics with negative $\Delta\sigma$, above and below some frequency v_l [6, 7]. Both of these regimes are

characterized by a field threshold. At the threshold of the low-frequency branch a set of convective rolls aligned approximately parallel to the undistorted director $\mathbf{n}_0$ ('longitudinal' domains) are found. The width of these rolls is comparable to the sample thickness. In the high-frequency regime a set of linear rolls directed arbitrarily in the medium develops at the threshold. The width of these rolls is much less than the sample thickness.

The Helfrich [1] and Orsay [2, 3] models require that the parameter

$$\zeta^2 = \left(1 - \frac{\sigma_\perp}{\sigma_\parallel}\frac{\varepsilon_\parallel}{\varepsilon_\perp}\right)\left(1 + \frac{\alpha_2}{\eta}\frac{\varepsilon_\parallel}{\Delta\varepsilon}\right),$$

where $\eta = \frac{1}{2}(\alpha_4 + \alpha_5 - \alpha_2)$, should be greater than 1 for E.H.D. instabilities to develop. This criterion is *not* satisfied by the materials mentioned above. However, we find that when the flexoelectric terms are included, E.H.D. instabilities can be obtained even in such materials. In our calculations we have doubled the values of K_1, K_2, K_3, e_1 and e_3, listed in the table, since the values of these parameters are known to be enhanced close to the smectic–nematic transition point. Further, near this temperature, it is also known that the viscosity coefficient α_3 changes sign [6, 18]. We assume that $\alpha_3 = 0.5\,\mathrm{P}$ and $\Delta\sigma = -3 \times 10^{-11}\,\mathrm{ohm}^{-1}\,\mathrm{cm}^{-1}$. We note here that K_1 and K_3 of 40·8 are found to double within 2–3° of the N–S transition point [19, 20], and $\Delta\sigma$ changes sign at around the same temperature. The 'longitudinal' E.H.D. rolls are also obtained, without increasing the values of the elastic constants or the flexoelectric coefficients, by changing $\Delta\varepsilon$ to -0.2. We do not find solutions corresponding to the conduction regime, but those corresponding to the dielectric regime do exist. The threshold field is found to be minimized for $q = 0$. Therefore we use the Helfrich criterion, $q = \pi/d$, at the threshold, d being the sample thickness. Thus the width of the rolls is comparable to the sample thickness, as found experimentally for the low-frequency regime in these materials. Since the solutions correspond to the dielectric regime, the instability is characterized by a field threshold. Further, at the threshold, $\alpha \approx 1.34\,\mathrm{rad}$ and is practically independent of the frequency, i.e. the rolls are nearly 'longitudinal'. The frequency dependence of the threshold field is similar to that in the dielectric regime of materials with positive $\Delta\sigma$ (see figure 15). It is clear that in this case the space-charge formation is due entirely to the flexoelectric effect, which also accounts for the large value of α. The light-scattering experiments of Goscianski [6] indicate that the curvature of the director field oscillates in such rolls, confirming that the medium is in the dielectric regime.

We do not find solutions corresponding to the high-frequency regime where $q \gg \pi/d$. Here it should be noted that at high frequencies the experimental value of $\Delta\sigma$ will have a positive contribution from the dielectric loss associated with the relaxation of $\varepsilon_\parallel$. As shown by Goossens [21], this contribution can cause E.H.D. instabilities at relatively high frequencies. Experimentally, even dynamic scattering has been seen at frequencies of about 50 kHz, at sufficiently high voltages, apparently owing to this contribution [22, 23]. This also means that the instability at threshold is hydrodynamic in origin.

In nematics with a negative $\Delta\sigma$ at low frequencies it is possible that the effective conductivity anisotropy at high frequencies is positive owing to the contribution from the dielectric loss of $\varepsilon_\parallel$. These materials can then be expected to show a high-frequency instability similar to the dielectric regime in nematics with positive $\Delta\sigma$. This can account for the experimental observation that the high-frequency instability in these materials goes over smoothly to the 'standard' dielectric regime as the temperature is increased.

Thus the inclusion of flexoelectric terms in the one-dimensional model of E.H.D. instabilities in nematics leads to a reasonable explanation of several observations that were not adequately accounted for by earlier models.

References

[1] HELFRICH, W., 1969, *J. chem. Phys.*, **51**, 4092.
[2] DUBOIS-VIOLETTE, E., DE GENNES, P. G., and PARODI, O., 1971, *J. Phys., Paris*, **32**, 305.
[3] SMITH, I. W., GALERNE, Y., LAGERWALL, S. T., DUBOIS-VIOLETTE, E., and DURAND, G., 1975, *J. Phys., Paris*, **36**, C1–237.
[4] RIBOTTA, R., JOETS, A., and LEI, L., 1986, *Phys. Rev. Lett.*, **56**, 1595.
[5] ORSAY LIQUID CRYSTALS GROUP, 1971, *Molec. Crystals liq. Crystals*, **12**, 251.
[6] GOSCIANSKI, M., 1975, *Philips Res. Rep.*, **30**, 37; see also GOSCIANSKI, M., and LEGER, L., 1975, *J. Phys., Paris*, **36**, C1–231.
[7] BLINOV, L. M., BARNIK, M. I., LAZAREVA, V. T., and TRUFANOV, A. N., 1979, *J. Phys., Paris*, **40**, C3–263.
[8] MADHUSUDANA, N. V., RAGHUNATHAN, V. A., and SUMATHY, K. R., 1987, *Pramana J. Phys.*, **28**, L311.
[9] RAGHUNATHAN, V. A., and MADHUSUDANA, N. V., 1988, *Pramana J. Phys.*, **31**, L163.
[10] MADHUSUDANA, N. V., and RAGHUNATHAN, V. A., 1988, *Molec. Crystals liq. Crystals Lett.*, **5**, 201.
[11] MEYER, R. B., 1969, *Phys. Rev. Lett.*, **22**, 918.
[12] BOBYLEV, YU. P., and PIKIN, S. A., 1977, *Soviet Phys. JETP*, **45**, 195.
[13] HIRATA, S., and TAKO, T., 1981, *Jap. J. appl. Phys.*, **20**, L459.
[14] RAGHUNATHAN, V. A., and MADHUSUDANA, N. V. (to be published).
[15] HIRATA, S., and TAKO, T., 1982, *Jap. J. appl. Phys.*, **21**, 675.
[16] ZIMMERMANN, W., and KRAMER, L., 1985, *Phys. Rev. Lett.*, **55**, 402.
[17] THOM, W., ZIMMERMANN, W., and KRAMER, L., 1988, Preprint.
[18] SKARP, K., CARLSSON, T., LAGERWALL, S. T., and STEBLER, B., 1981, *Molec. Crystals liq. Crystals*, **66**, 199.
[19] LEGER, L., 1973, *Phys. Lett. A*, **44**, 535.
[20] D'HUMIERES, D., and LEGER, L., 1975, *J. Phys., Paris*, **36**, C1–113.
[21] GOOSSENS, W. J. A., 1972, *Phys. Lett. A*, **40**, 95.
[22] DE JEU, W. H., GERRITSMA, C. J., VAN ZANTEN, P., and GOOSSENS, W. J. A., 1972, *Phys. Lett. A*, **39**, 355.
[23] DE JEU, W. H., and LATHOUWERS, T. W., 1974, *Molec. Crystals liq. Crystals*, **26**, 235.